

Article

C–O Stable Isotopes Geochemistry of Tunisian Nonsulfide Zinc Deposits: A First Look

Hechmi Garnit ¹, Maria Boni ^{2,*}, Giuliana Buongiovanni ², Giuseppe Arfè ², Nicola Mondillo ², Michael Joachimski ³, Salah Bouhlel ¹ and Giuseppina Balassone ²

¹ Mineralogy and Geochemistry Research Group, Mineral Resources and Environment Lab (LR01ES06), Faculty of Sciences of Tunis, University of Tunis El Manar, 2092 Tunis, Tunisia; garnit1hechmi@yahoo.fr (H.G.); Salah.bouhlel@fst.rnu.tn (S.B.)

² Dipartimento di Scienze della Terra, dell'Ambiente e delle Risorse, Università degli Studi di Napoli Federico II, Complesso Universitario di Monte S. Angelo, Via Cintia, 80126 Napoli, Italy; giulianabuongi@gmail.com (G.B.); pepparfe@gmail.com (G.A.); nicola.mondillo@unina.it (N.M.); balasson@unina.it (G.B.)

³ GeoZentrum Nordbayern, University of Erlangen-Nuremberg, Schlossgarten 5, 91054 Erlangen, Germany; michael.joachimski@fau.de

* Correspondence: boni@unina.it; Tel.: +39-081-2535068

Received: 30 November 2017; Accepted: 3 January 2018; Published: 9 January 2018

Abstract: A preliminary C–O stable isotopes geochemical characterization of several nonsulfide Zn–Pb Tunisian deposits has been carried out, in order to evidence the possible differences in their genesis. Nonsulfide ores were sampled from the following deposits: Ain Allegua, Jebel Ben Amara, Jebel Hallouf (Nappe Zone), Djebba, Bou Grine, Bou Jaber, Fedj el Adoum, Slata Fer (Diapir Zone), Jebel Ressay, Jebel Azreg, Mecella (North South Axis Zone), Jebel Trozza, Sekarna (Graben Zone). After mineralogical investigation of selected specimens, the C–O stable isotopic study was carried out on smithsonite, hydrozincite, cerussite and calcite. The data have shown that all the carbonate generations in the oxidized zones of Ain Allegua and Jebel Ben Amara (Nappe Zone), Bou Jaber, Bou Grine and Fedj el Adoum (Diapir Zone), Mecella and Jebel Azreg (North South Zone) have a supergene origin, whereas the carbonates sampled at Sekarna (Graben Zone) (and in limited part also at Bou Jaber) precipitated from thermal waters at moderately high temperature. Most weathering processes that controlled the supergene alteration of the Zn–Pb sulfide deposits in Tunisia had probably started in the middle to late Miocene interval and at the beginning of the Pliocene, both periods corresponding to two distinct tectonic pulses that produced the exhumation of sulfide ores, but the alteration and formation of oxidized minerals could have also continued through the Quaternary. The isotopic characteristics associated with the weathering processes in the sampled localities were controlled by the different locations of the sulfide protores within the tectonic and climatic zones of Tunisia during the late Tertiary and Quaternary.

Keywords: nonsulfide deposits; Tunisia; C–O stable isotopes; mineralogy; paleoclimate

1. Introduction

North-Central Tunisia is part of the Alpine Atlas mountain ranges, extending toward the west through Algeria and Morocco along the Mediterranean coast. In this mountain belt, Triassic to upper Miocene carbonate rocks host numerous Zn–Pb sulfide deposits, which genetically represent varieties of the typical Mississippi Valley-type (MVT) ores [1–5]. The nonsulfide Zn–Pb deposits of Tunisia have not been investigated since the pioneering works of [6–9]. These authors reported that Pb–Zn sulfide ores overlain by oxidized gossans and caps were widely distributed throughout the Tunisian belts [6–9]. Smithsonite, hemimorphite and hydrozincite were recognized as the principal zinc minerals, directly

replacing the hypogene sulfide bodies in oxidation zones. For this reason, these authors proposed that all of the Tunisian nonsulfide ores were formed through supergene processes associated with weathering. Even though recent papers (e.g., [10]) have shown that C–O stable isotopes can be useful to better identify the nature of the fluids precipitating nonsulfide mineralizations, stable isotopes data on Zn and Pb carbonates from Tunisian nonsulfide deposits have been lacking so far [4,5].

In this paper, we present the results of a preliminary C–O stable isotopes' geochemical study on carbonate minerals occurring in several nonsulfide Zn–Pb Tunisian deposits, in order to evidence possible differences in their genesis. The studied samples originate from deposits located in the four tectonic-metallogenic zones of North-Central Tunisia: Nappe Zone, Diapir Zone, North-South Axis Zone and Graben Zone. The selected deposits are: Ain Allegua, Jebel Ben Amara, Jebel Hallouf (Nappe Zone), Djebba, Bou Grine, Bou Jaber, Fedj el Adoum and Sлата Fer (Diapir Zone), Jebel Ressayas, Jebel Azreg, Mecella (North South Axis Zone) and Jebel Trozza, Sekarna (Graben Zone).

2. Geological, Climatic and Metallogenic Setting of Tunisia

2.1. Regional Geology

The Atlassic domain of Northern Tunisia is a part of the Maghrebide Chains that form the North African margin and extend along the Mediterranean coast through Morocco, Algeria and Tunisia. The uppermost crust in the area is comprised of a ca. 12,000 m-thick Phanerozoic sedimentary sequence that has been deformed by the multiphase Meso-Cenozoic Alpine orogeny. In Tunisia, the Atlassic chains include the Tellian Thrust belt and the Atlassic Foreland Fold belt. The Tellian Thrust belt is characterized by dominantly SE-verging and NE-SW striking thrust sheets that were tectonically displaced to the southeast during the Middle Miocene and are composed of stacked and sheet-like Eocene limestone and marl successions overlain by Oligocene-Miocene siliciclastic sediments [11]. The complex Atlassic foreland fold belt includes from north to south: (i) the Diapir Zone (Mejerda Valley) with salt extrusions throughout Jurassic-Miocene strata, (ii) the Graben Zone (or central Atlas) with large-scale NE-SW striking folds that show Cretaceous-Eocene strata intersected by NW-SE-directed Mio-Pliocene troughs [12] and (iii) the North-South Axis Zone extending to the southeast, which displays folds transected by reactivating shear-faults and that separates the Eastern Atlas from the Sahel [12,13].

2.2. Current and Past Climatic Conditions

The northern coast of Africa currently experiences a Mediterranean climate, which mostly depends on the position of the Intertropical Convergence Zone (ITCZ) [14]. The ITCZ controls in large part the seasonal variability of the precipitation patterns and determines distinct atmospheric circulation systems in most of the African regions (e.g., northern Africa vs. southern Africa) [15–17]. The north Atlantic and the El Niño Southern Oscillations [18,19] largely influence the interannual to interdecadal variability in the northern African regions. This variability has persisted for several hundred years, and it could be traced also in Greenland ice cores' data [20].

During the Cenozoic, northern Africa experienced several climate changes [17,21–23] and only after middle Miocene, when the present-day climatic system was established, the oceanic circulation pattern became similar to the modern one [24,25]. The most important weathering periods in northern Africa coincide with the middle to late Miocene and with the middle Pliocene. During the Miocene, weathering phenomena increased in northern Africa [26], and the “Zeit Wet Phase” (7.5–5.5 Ma [27]) began. Pollen records and the parameter elevation regression on independent slopes model (PRISM) indicate that also during the middle Pliocene (4.5–3 Ma), North Africa was wetter and warmer relative to the current climate conditions [28–30]. This part of Africa became definitely drier after 2.8 ± 0.2 Ma, as indicated by pollen [28] and dust records observed in West and East Africa [31–33]. However, minor wet periods also occurred during the Holocene, when the “African Humid Period” (15–5 ka) affected the northern regions [34,35]. Early to middle Holocene climate conditions were more humid than the modern ones [36–38].

2.3. Distribution and General Characteristics of Zn-Pb Ore Deposits

Most known Zn-Pb-(Ba, Sr, F) ore deposits from North-Central Tunisia are shown in Figure 1. Each of these deposits contains low to medium size resources with 1–8 Mt at about 5–15% Zn + Pb. The ores are hosted in carbonate rocks of various ages, ranging from Triassic to Mio-Pliocene. In terms of tectonic setting, host rock ages and paragenesis, the sulfide deposits in this part of Tunisia are subdivided into five sub-types [1,3,5,39]:

- Group 1: Zn-Pb mineralizations subdivided into two sub-groups: (a) polymetallic veins (Pb-Zn-Cu-As-Hg) along faults and (b) clastic-dominated Zn-Pb deposits within Late Miocene siliciclastic rocks and lacustrine limestones. Most of these deposits are located in the Nappe Zone of the Tellian Atlas (e.g., Jebel Hallouf, Sidi Bouaouane, Sidi Driss, Djebba) [1,40].
- Group 2: Pb-Zn-(Sr) stratabound replacement-type deposits within Triassic evaporite solution breccias at the contact zones of salt diapirs, salt glaciers or salt sheets and the surrounding Cretaceous to Miocene rocks. Most deposits (e.g., Fedj el Adoum, Bou Grine, Kebbouch, Bou Khil, Garn Halfaya, Zag Ettir, Doggra) are located within the Diapir Zone, some others (e.g., Ain Allegua, Aguiba, Bechateur) in the Nappe Zone ([2,41]).
- Group 3: Zn-Pb vein-type and stratabound replacement deposits crosscutting Cretaceous limestones and subordinately Oligocene-Miocene sandstones in the vicinity of Triassic salt diapirs (e.g., Oued el Jebbs, Kebbouch, Bou Khil, El Akhouat, Koudiat Safra deposits) [1,4,39,42–44].
- Group 4: Ba-F-(Pb-Zn) stratabound replacement-type and cavity-filling deposits developed within Aptian platform/reef limestone near salt diapirs involving Triassic evaporites. Most deposits are located in the western area of the Diapir Zone and the Graben Zone. Two distinct mineral assemblages occur: Subgroup 4a with Ba-F-(Pb-Zn) (e.g., Mesloula, Mzouzia, Belkif deposits in Algeria; and Bou Jaber in Tunisia); and Subgroup 4b consisting of Ba-(Pb-Zn) deposits (e.g., Slata Fer, Hamra, Ajred, Trozza) [39,45,46]. A Ba-(Pb-Zn) mineralization is also present in early Eocene phosphorite-rich rocks (Sekarna) [47].
- Group 5: stratabound and vein-type F-Ba-(Pb-Zn) deposits occurring in the upper parts of two Jurassic carbonate platform units: the Oust Limestone (Early Jurassic) hosts the El Khol, Stah and Hammam Jedidi deposits, while the Ressay Limestone (Late Jurassic) hosts the Mecella, Ressay, Hammam Zriba and Sidi Taya deposits.

The mineralogy of Tunisian Zn-Pb sulfide deposits includes fine-grained and banded collomorphic sphalerite, honey- to brown-colored sphalerite, coarse-grained massive galena and marcasite/pyrite. The gangue minerals are calcite, barite and celestite. Some deposits are fluorite-rich and sulfide-poor. The ores occur in limestones, rarely in dolostones. Hydrothermal alteration of the carbonate host rock includes silicification, dolomitization and ankeritization and may vary within a single deposit. These common features allowed classifying the Tunisian sulfide deposits as Mississippi Valley-type mineralizations [1,3–5,39,41]. Since the Tunisian Zn-Pb ores replace and crosscut Triassic to Mio-Pliocene host-rocks, they are considered to be genetically associated with the Alpine tectonic activity [8,39], which started in the Late Cretaceous in this region and reached its maximum with two successive phases in the middle Miocene and late Miocene-Pliocene [48,49]. The Middle Miocene tectonic events were probably the most important mechanism for expulsion and circulation of orogenic-related metal- and hydrocarbon-bearing brines. Thrusting, regional NE-SW and NW-SE deep faults, salt diapirs and unconformities acted as pathways for the fluid flow [1,3]. During the Pliocene to Quaternary interval, the Atlas chain was subjected to post-orogenic relaxation, emersion and erosion. In the Atlasic foreland domain, Pliocene reactivation of transpressional movements created several transverse NW-SE-trending grabens [50,51], which intersect and cut across the SW-NE-oriented folds and salt diapirs. One of the effects of these late tectonic phases was the exposure to weathering of the sulfide ores and the formation of nonsulfides in the oxidation zone.

3. Nonsulfide Ore Deposits and Their Sulfide Protores: Geological and Mineralogical Background

3.1. Nappe Zone

The Ain Allegua orebodies (Figure 2) are stratabound and characterized by open-space and karst-filling features. They have been considered in the past as cap rock-type Pb-Zn-(Sr) mineralizations, hosted in Triassic breccias along Miocene thrust detachments [8]. More recently, however, several stratabound Pb-Zn-As-Sb orebodies were also detected in late Miocene continental sediments in the same area [3].

The Jebel Ben Amara Pb-Zn-(Ba) deposit occurs in Campanian carbonates and is characterized by sub-vertical veins and lenses [8]. The main gangue mineral is calcite. In the nonsulfide part of the deposit, the ore assemblage mainly consists of banded and massive smithsonite (30–40% Zn), associated with black and fine-grained cerussite [8].

The mineralized bodies of the Jebel Hallouf mine are hosted by Campanian–Maastrichtian limestones. The deposit exhibits two styles of mineralization: cavity- and vein-filling [52–54]. Karst-fillings are developed at the northern side of the Jebel Hallouf anticline. Most minerals are found as incrustations on cavity floors, walls and ceilings. They also occur within layered sediments issued from the reworking of the former deposits, as well as stalactites. The mineral assemblage of the vein-filling type consists of galena, sphalerite and jordanite. Cerussite and smithsonite (37% Zn) are the main alteration products [53]). Four mineralized areas were recognized over 3 km [8]: (i) the Calamine district, comprising a series of mineralized pockets and veins with smithsonite; (ii) the West district, comprising two EW-trending vein zones with a quite irregular mineralization; (iii) the Attilio district, which represents the principal economic ore and consists of four veins; (iv) the Palmier district, consisting of a series of cerussite-rich fractures.

3.2. Diapir Zone

The Djebba deposit is located in Neogene sediments and in Triassic dolostone (Figure 1). The main ore bodies are at Bou Touil, Laffina and Goraa. The Pb orebody of Bou Touil is a stockwork type mineralization hosted in Cenomanian-Turonian limestones. At Jebel Goraa sub-vertical veins with Fe-smithsonite and vanadinite occur in Eocene limestones [55].

The Fedj el Adoum deposit is located in the NE-SW-trending El Kef rift system (Figure 1) that started forming during Late Jurassic and reached its maximum activity in the Cretaceous (Aptian to Cenomanian). Salt diapirism occurred during the late Aptian and continued from the Late Cretaceous to recent [39,56]. The Zn-Pb occurrences are located where the NW-SE trending faults intersect the SE margins of the salt diapirs [41]. Their distribution is interpreted to reflect a hydrothermal fluid flow along tectonic lines. Sulfides are hosted in the so-called Transition zone or cap-rock [2,39,41]. There are at least four mineralization types [41] called: Zn-rich ore, zebra calcite (barren), Pb-rich ore and native sulfur. The Zn-rich ore consists of Zn >> Pb, stratabound, lens-shaped orebodies, accounting for 80% of the ore resources at Fedj el Adoum. The mineralization occurs as replacement of dolostone or as open space filling. Alternating dark- and cream-colored bands are common. The dark bands consist of Triassic dolostone fragments, whereas the cream-colored bands consist of collomorph sphalerite. The Zebra calcite consists of irregular patches with “zebra” structures, consisting of mm- to cm-scale alternations of dark and white calcite. The Pb-rich ore is represented by Pb >> Zn, veins, stockworks or massive mineralization. This type accounts for 20% of the Fedj el Adoum resources. Post-sulfide sparry calcite has filled the remnant porosity.

The Bou Grine Zn-Pb deposit is located on the northeastern flank of the Jebel Lorbeus Triassic evaporites dome, in the southern part of the Diapir Zone [8,12,42,57] (Figure 1). This is the largest known lead-zinc deposit in Tunisia [42], mined from 1993–2005 [4]. At Bou Grine, there are five bodies designated in order of their discovery as F1, F2, F3, F4 and F5 and described by [3,42,43] and [4]. The orebodies are hosted either in the Cenomanian-Turonian limestones of the Bahloul Formation or

at the transition zone between Cretaceous marly limestones/dolostones and the salt diapir intrusion. Most nonsulfide ores occur in the F1 orebody.

The Bou Jaber Ba-Fe-Pb-Zn deposit is located near the Algerian border, in the western part of the Diapir Zone (Figure 1). Lead, silver and zinc were initially exploited in this deposit, while barite and fluorite were mined only later [5]. The mineralization (hosted in late Aptian carbonates, along the flanks of a northwest-dipping salt diapir) consists of several small- to medium-size bodies, which are fault and unconformity controlled. The rich ores form three roughly vertical bodies in the central part of the deposit. From the outer part to the core, most orebodies have a sulfide-rich zone, a mixed barite/sulfide zone and a late barite-rich zone [5].

The Slat Fer orebody consists of karst fillings in Aptian reef limestone (Figure 1), intruded by the salt diapir of Ben Gasseur. The primary ore association consists of hematite, galena and barite with ankerite and calcite gangue [5,8]. Rare copper occurs in the form of bertholite [8]. Manganese occurs as cesarolite. Nonsulfide minerals commonly occur as the alteration of the primary sulfides.

3.3. Graben Zone

The Jebel Trozza deposit (Figure 2) consists of large veins (13 m thick, 150 m high, length over 1 km) containing galena, as well as small cerussite veins. Zinc and lead nonsulfides occur in Fe-rich clays and in zones enriched with barite and galena in late Aptian dolomitized limestones [8].

The Sekarna deposit is located in Central Tunisia, in the Tertiary Graben Zone, about 220 km southwest of Tunis, northwest of the structural domes (Diapir Zone) and southeast of the Central Tunisian Carbonate Platform (Figure 1). The Sekarna deposit consists of two different orebodies, called Saint Pierre and Saint Eugène. The Saint Eugène orebody is hosted in the early Eocene dolomite of the Metlaoui Group, whereas the Saint Pierre orebody is hosted in the Campanian-Maastrichtian limestone of the Abiod Formation. Both occurrences contain mixed sulfide to nonsulfide ores [47]. The Saint Pierre orebody is a stratiform Zn-Pb-(Ba) sulfide mineralization (10–13% Zn, 3–5% Pb), hosted by unusually hard, massive, phosphatic–glauconitic Ypresian (early Eocene) microconglomerates [47], consisting of sphalerite (90% of the ore), galena, Fe sulfides and barite. The upper part of this orebody is fully oxidized and contains Cd-rich smithsonite, and Fe-oxy-hydroxides [47]. Massive galena (3–14%) and supergene nonsulfide Zn minerals, such as Fe-poor smithsonite (<2 wt % FeO), hemimorphite and hydrozincite, also occur in karstic cavities developed in late Cretaceous carbonate rocks. Colloform cerussite and anglesite are intergrown within fractures in galena and along grain boundaries [47]. The Saint Eugène orebody is hosted in dolomitic limestones, associated with two major NE-SW-trending faults. The main Zn mineral in the orebody is smithsonite, whereas hemimorphite, hydrozincite, cerussite and anglesite are minor constituents. Iron-oxy-hydroxides are very common. Calcite is commonly associated with smithsonite [47].

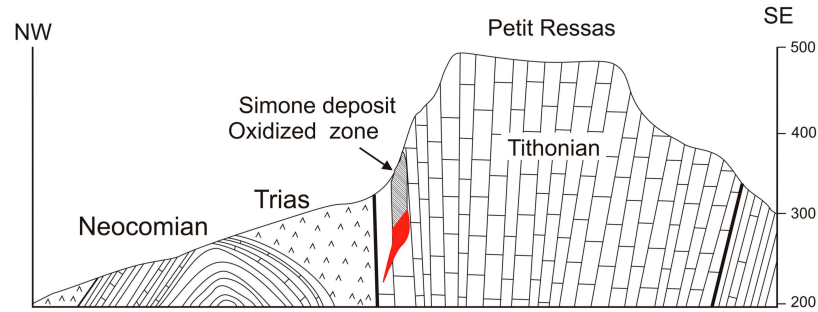
3.4. North South Axis Deposits

The Mecella deposit (Figure 2) is located in the Zaghouan Fluorite district [7,9,58–61]. This area is characterized by several outcrops of Jurassic limestones, surrounded by Early Cretaceous successions of marly limestone. The Jurassic massifs are bordered to the East by the NE-SW “Zaghouan Fault”, locally injected by Triassic salt diapirs [13,62]. The mineralization is stratabound and occurs as lenses and irregular karstic bodies at the unconformable contact between Late Jurassic and Valanginian (Early Cretaceous) strata [63] (Figure 1). The primary mineral association consists of fluorite, celestite-barite, quartz, sphalerite and galena [39].

The Jebel Ressas deposit (Figure 2) also belongs to the Zaghouan Fluorite district. The base metal ores are hosted in Early Jurassic reef limestones (Figure 1) of the Oust Formation and in the Late Jurassic (Tithonian) Ressas Formation. Most authors agree with the attribution of the deposit to the Mississippi Valley-type (MVT) [39,60,61]. The Zn-Pb sulfide deposit occurs within sub-vertically dipping strata [8] in the form of: lens-shaped pods at the contact of the Tithonian Ressas Formation and Triassic limestones (Petit Ressas deposit, Simone ore) and open-space fillings (NS trending fractures, columnar orebodies and tectonic breccias) with Pb-Zn calamine ores in Tithonian limestones (Grand Ressas deposit). The mineralization consists of Zn and Pb nonsulfides with remnants of galena and sphalerite. The mineralogy varies depending on the position of the respective bodies in relation to the water table. Above the water table, the deposits contain abundant secondary minerals consisting of carbonates (cerussite, hydrozincite), silicates (hemimorphite) and Fe-oxy-hydroxides. Other accessory minerals such as smithsonite, Pb-strontianite, barite, celestite, willemite and zincite have been also recognized.

The Jebel Azreg mineralized complex is located in the Hamama Jedidi district. This district contains at least ten fluorite-rich ore deposits that form the eastern part of the Tunisian fluorite province [9,59]. The main deposits are located at Jebel Hammam and Jebel Azreg. The mineralization is associated with a diapir of Triassic evaporites that intruded Jurassic platform carbonates and Cretaceous limestones and marls. The mineralization occurs in veins and breccia zones crosscutting Jurassic platform carbonates or along tectonic breccias in the contact zones between Triassic, Jurassic or Cretaceous strata [39,59]. The primary minerals are galena, sphalerite, chalcopyrite and tennantite-tetrahedrite. The gangue consists of barite, celestite and calcite. Dolomitization and silicification of the host limestone are common. At Jebel Azreg, supergene minerals include Pb-bearing sulfates, carbonates, phosphates and arsenates. Zn-bearing carbonates and hydrosilicates also occur.

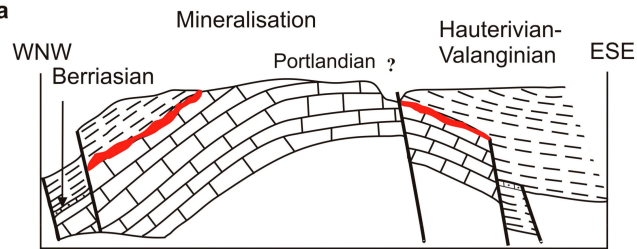
Jebel Ressas



Ain Allegua



Mecella



Jebel Trozza

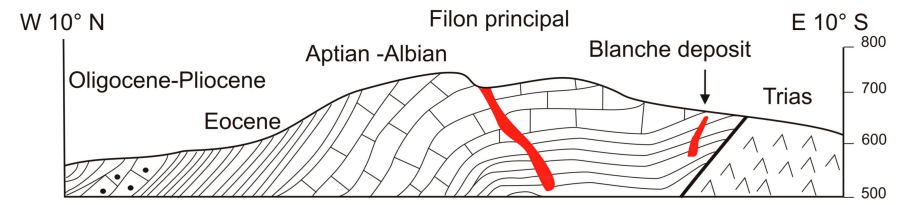


Figure 2. Some cross-sections of the studied deposits: Jebel Ressas, Ain Allegua and Jebel Trozza are from [7]; Mecella is from [60].

4. Materials and Methods

Twenty-four samples from nonsulfide Zn deposits, located in the four tectonic-metallogenic zones of North-Central Tunisia, have been selected for mineralogical analysis. The considered localities and the list of collected samples are reported in Table 1.

X-ray powder diffraction (XRPD) analyses have been carried out on the samples, after crushing and grinding, with a diffractometer Seifert-GE ID 3003 (Dipartimento di Scienze della Terra, dell'Ambiente e delle Risorse—DiSTAR, Università degli Studi di Napoli Federico II, Napoli, Italy), with a Cu anode, tension 40 kV, electric current 30 mA, time 5 s/step, step scan 0.05° 2 theta, divergence slit 2 mm, anti-scatter slit 0.5 mm and Ni filter. XRD spectra were processed by RayFlex[®] software, supplied by the Seifert-GE diffractometer (DiSTAR, Università degli Studi di Napoli Federico II, Napoli, Italy).

Scanning electron microscope (SEM) analyses were carried out with a Jeol JSM 5310, supported by the INCA-EDS 4.08 Energy Dispersive Microanalysis System (DiSTAR, Università degli Studi di Napoli Federico II, Napoli, Italy), working with: sensitivity 10,000 c/s/Na, beam current ~ 0.5 Na, measure time 50 s, 15 keV (all elements), detection limit 1000 ppm.

Carbon and oxygen stable isotope analyses were performed on 15 smithsonites, 2 hydrozincites, 2 cerussites, 6 supergene calcites, 3 hydrothermal calcites, 9 specimens of the host limestone and 7 of the host dolomite, subsampled (subsample IDs are given in Table 2) from the 24 specimens collected on site for this study (Table 1). The analyses were carried out at the University of Erlangen-Nuremberg (Erlangen, Germany). Pure carbonate samples were collected by mechanical hand picking directly from the specimens. All samples were reacted with 100% phosphoric acid at 70 °C, using a Gasbench II connected to a ThermoFisher Delta V Plus mass spectrometer (University of Erlangen-Nuremberg, Erlangen, Germany). Carbon and oxygen isotope values are reported in per mil relative to V-PDB (Vienna-Pee Dee Belemnite) and V-SMOW (Vienna-Standard Mean Oceanic Water), respectively. Reproducibility and accuracy were monitored by replicate analysis of NBS19 and LSVEC laboratory standards calibrated by assigning $\delta^{13}\text{C}$ values of +1.95‰ to NBS19 and -46.6 ‰ to LSVEC and $\delta^{18}\text{O}$ values of -2.20 ‰ to NBS19 and -23.2 ‰ to NBS18. Reproducibility for $\delta^{13}\text{C}$ and $\delta^{18}\text{O}$ was $(\pm 1\sigma)$ and $(\pm 1\sigma)$, respectively. Oxygen isotope values of dolomite, cerussite and smithsonite were corrected using the phosphoric acid fractionation factors given by [64–67]. Due to the absence of the proper phosphoric acid fractionation factors, oxygen isotope values of hydrozincite were corrected by using the smithsonite equation given by [67].

Table 1. Sample list and mineralogy of the studied samples.

Zone	Deposit	Sample ID	Host Rock		Hypogene Mineralization							Supergene Mineralization												
			cal	dol	sph	gal	py	ccp	h cal	dol	qz	fl	cel	sm	hem	ce	hydr	angl	goe	dscz	brc	mlc	s cal	kln
Nappe Zone	Ain Allegua	AA				X						X		X								X		
	Jebel Ben Amara	JBA											X									X		
	Jebel Hallouf	JH			X	X	X		X															
Diapir Zone	Djebba	DJ																X	X			X		
	Fedj El Adoum	FEA TD		X	X	X							X	X				X					X	
	Bou Grine	BG 1											X										X	
		BG 2 BF		X									X										X	
	Bou Jaber	BJ 1		X										X									X	
		BJ 2				X	X			X						X								
	Slata Fer	SF								X														X
SFH			X																					
Graben Zone	Jebel Trozza	JT		X		X						X			X	X	X			X			X	
	Sekarna	SK 1-St. Pierre												X	X									
		SK 2-St. Pierre												X										
		SKH 1 SKH 2		X		X																		
Mecella	MC											X	X		X							X	X	
	MCN											X		X										
N-S Axis Zone	Jebel Ressay	JR	X		X	X			X	X	X				X			X				X		
		JRH	X																					
		LC	X																					
Jebel Azreg	JA						X	X	X	X	X			X		X				X	X			

Note: sph = sphalerite, gal = galena, py = pyrite, ccp = chalcopyrite, h cal = hydrothermal calcite, dol = dolomite, qz = quartz, fl = fluorite, ba = barite, cel = celestite, sid = siderite, sm = smithsonite, hem = hemimorphite, ce = cerussite, hydr = hydrozincite, angl = anglesite, goe = goethite, dscz = descloizite, brc = brochantite, mlc = malachite, s cal = calcite, kln = kaolinite, gyp = gypsum. X means that the mineral is present in the considered sample.

Table 2. C and O isotopes data of carbonates from the considered Zn-Pb deposits.

Zone	Deposit	Sample ID	Subsample ID	Mineral	Description	$\delta^{13}\text{C}$ ‰ (V-PDB)	$\delta^{18}\text{O}$ ‰ (V-SMOW)	Reference
Nappe Zone	Ain Allegua	AA	AA ISO 1	ce	cerussite crust above galena	−12.21	16.88	This study
	Jebel Ben Amara	JBA	JBA ISO 3	sm1	concretionary smithsonite	−7.83	25.37	This study
			JBA ISO 2	sm2	concretionary smithsonite	−8.49	25.76	This study
			JBA ISO 1	s cal	supergene calcite	−11.24	25.64	This study
	Jebel Hallouf	JH	JH ISO 1	h cal	hydrothermal calcite gangue associated with galena	5.00	19.87	This study
			JH ISO 3	h cal	hydrothermal calcite gangue associated with galena	5.94	23.60	This study
Diapir Zone	Djebba	DJ	DJ ISO 1	s cal	supergene calcite	−10.10	25.04	This study
	Fedj El Adoum	FEA TD Literature	FEA ISO 1	sm	smithsonite associated with sulfides	−5.50	26.86	This study
			FEA ISO 2	sm	concretionary smithsonite with goethite	2.11	25.12	This study
			TD ISO 1	dol	Triassic dolomite host rock	0.84	26.44	This study
			dol * cal *	dol * cal *	banded dolomite in the host rock calcite from the contact zone	2.9–6.9 −8.1	28.6–30.1 31.6	[56] [56]
	Bou Grine	BG 1	BG ISO 5 BG ISO 3	sm2	smithsonite grey crust	−2.13	26.59	This study
				sm1 + sm2	smithsonite replacing the host rock + smithsonite grey crust	−1.40	27.29	This study
				s cal	supergene calcite following smithsonite	−5.27	22.68	This study
		BG 2	BG ISO 2 BG ISO 6 BG ISO 4	s cal	supergene calcite following smithsonite	−5	22.84	This study
				sm1	smithsonite replacing the host rock	−0.57	27.72	This study
BF		BF ISO 1 BF ISO 2	sm3	smithsonite reddish crust	1.92	24.29	This study	
			cal	Bahloul Formation (Cenomanian-Turonian) host rock	3.79	27.99	This study	
Literature	cal *	Bahloul Formation (Cenomanian-Turonian) host rock supergene calcite	2.50 −12–−4	30.81 19–25	This study [4]			
Bou Jaber	BJ 1 BJ 2 Literature	BJ ISO 1 BJ ISO 2	sm	smithsonite concretion	−2.87	25.09	This study	
			ce	cerussite crystals over galena vein	−5.62	12.09	This study	
			cal *	host rock	0.1–3.9	26.2–30.1	[5]	

Table 2. Cont.

Zone	Deposit	Sample ID	Subsample ID	Mineral	Description	$\delta^{13}\text{C}$ ‰ (V-PDB)	$\delta^{18}\text{O}$ ‰ (V-SMOW)	Reference	
	Slata Fer	SF	SF ISO 1	h cal	hydrothermal calcite	−2.52	20.4	This study	
		SFH	SFH ISO 1	dol	Aptian dolomite host rock	2.27	20.3	This study	
			SFH ISO 2	dol	Aptian dolomite host rock	2.52	24.98	This study	
Graben Zone	Jebel Trozza	JT	JT ISO 2	hydr	hydrozincite veinlet	−1.78	26.78	This study	
			JT ISO 3	dol	dolomite host rock	−1.3	21.16	This study	
	SK 1-St. Pierre	SK ISO 1	sm2	sm2	yellowish - white concretionary smithsonite-type 2	−5.13	22.17	This study	
					concretionary smithsonite-type 1	−4.55	21.96	This study	
	SK 2-St. Pierre	SK ISO 3	sm1	sm1	concretionary smithsonite-type 1	−4.76	22.44	This study	
					white concretionary smithsonite-type 2	−6.57	22.66	This study	
	Sekarna	SKH 1	SKH ISO 1	dol	Metlaoui Group (Eocene) host rock	1.50	20.93	This study	
					Abiod Formation (Campanian-Maastrichtian) host rock	2.01	22.73	This study	
	Literature	St. Eugene	sm *	dol *	-	−5.1	28.3	[47]	
					host rock	−2.3 to 2.6	21.6 to 23.9	[47]	
N-S Axis Zone	Mecella	MC	MC ISO 2	sm	banded smithsonite	−1.09	26.17	This study	
			MC ISO 1	s cal	banded calcite	−7.34	25.46	This study	
			MCN	MCN ISO 1	sm	colloform smithsonite	−6.49	25.83	This study
	Jebel Ressay	JR	JR ISO 1	JR ISO 2	s cal	concretionary calcite	−5.22	25.83	This study
					cal	carbonate host rock	1.53	23.84	This study
		JRH	JRH ISO 1	cal	cal	Jurassic carbonate host rock	2.51	26.33	This study
						Oust Formation (Early Jurassic) reef limestone host rock	2.26	21.06	This study
		LC	LC ISO 1	LC ISO 2	cal	Oust Formation (Early Jurassic) reef limestone host rock	2.20	22.5	This study
						post-ore calcite	0.9	24.8	[60]
	Literature	host rock	cal *	dol *	post-ore calcite	0.14 to 0.7	19.2 to 26.5	[60]	
					host rock	0.14 to 0.7	19.2 to 26.5	[60]	
	Jebel Azreg	JA	JA ISO 4	JA ISO 1	hydr	hydrozincite concretion in cavity	−10.76	25.52	This study
cal					calcite host rock	0.69	16.79	This study	
JA ISO 2					dol	dolomite host rock	2.55	17.21	This study

Note: sm = smithsonite, dol = dolomite, cal = calcite, hydr = hydrozincite; numbers (1, 2, etc.) were used if the paragenetic order was known; * = data from the literature. V-PDB = Vienna-Pee Dee Belemnite; V-SMOW = Vienna-Standard Mean Oceanic Water.

5. Results: Mineralogy and Stable Isotope Geochemistry of the Analyzed Samples

Sulfide remnants (sphalerite, galena and pyrite) have been recognized only in the samples from the Jebel Ressas, Jebel Hallouf, Bou Jaber, Fedj el Adoum and Ain Allegua deposits (Table 1). Sphalerite occurs as colloform aggregates and as void infillings and dissemination in the carbonate host rocks. Sphalerite is always associated with galena, which occurs in small veins or as euhedral crystals in vugs. Galena is partially or totally surrounded by cerussite rims. Commonly, pyrite has crystalline textures, but micro-spherulitic framboidal pyrite was also observed at Jebel Hallouf. The XRD and the SEM-EDS analyses allowed determining that among the oxidized minerals, smithsonite prevails over hemimorphite, cerussite and hydrozincite (Table 1, Figures 3–5). Minor amounts of desclozite, woodruffite, brochantite and malachite have been sporadically detected (Table 1). Accessory or gangue minerals are goethite, barite, fluorite, calcite, dolomite, quartz, kaolinite and gypsum (Table 1).

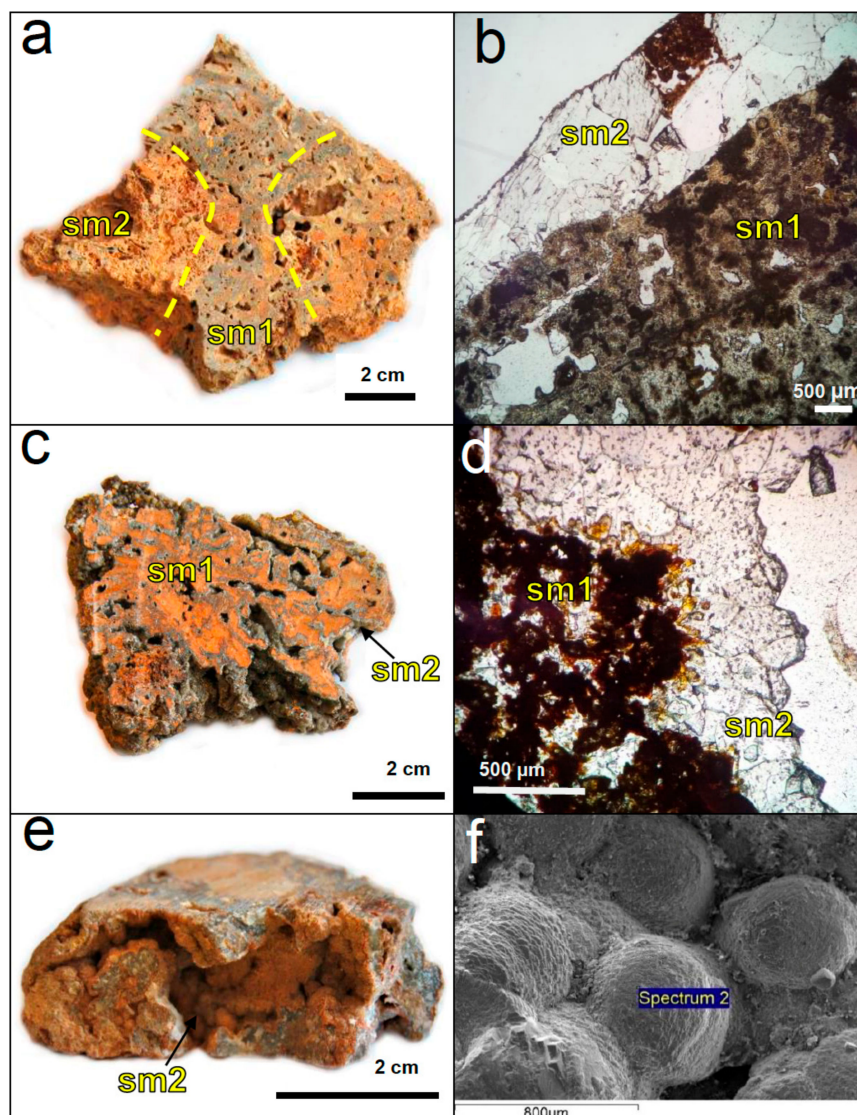


Figure 3. Jebel Ben Amara: (a) Hand specimen (JBA) with two generations of smithsonite. (b) Optical microscope image (N||) showing sm1 and sm2. Bou Grine: (c) Hand specimen (BG 1) with two generations of smithsonite. (d) Optical microscope picture (N||) showing the reddish host rock-replacive smithsonite (sm1) and the sm2 grey crust. (e) Hand specimen (BG 2) with sm2 grey crust overgrown by late concretionary reddish smithsonite (sm3). (f) SEM image of concretionary smithsonite from (e).

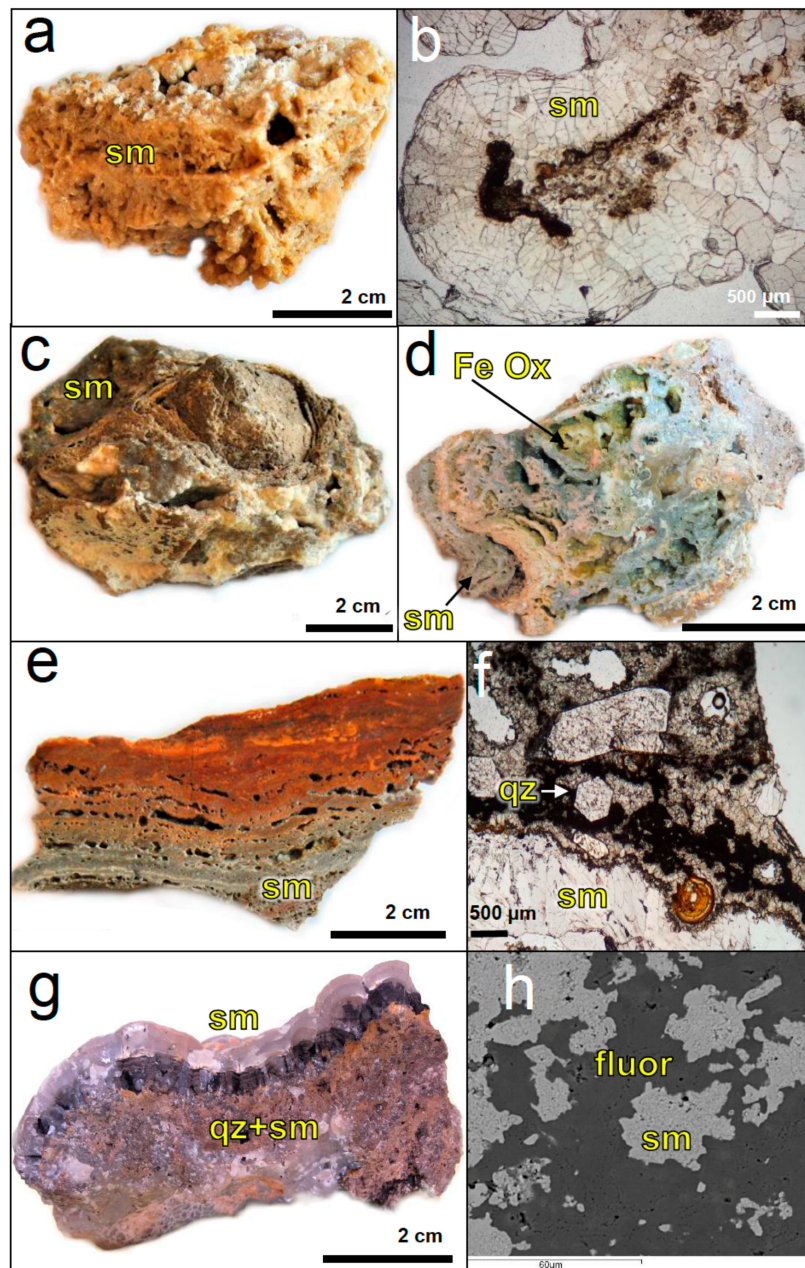


Figure 4. Sekarna: (a) Hand specimen (SK 1-St. Pierre) showing yellowish-white concretionary smithsonite (Type 2). (b) Optical microscope picture (N||) showing microtexture of concretionary smithsonite from (a). (c,d) White (Type 1) and grey (Type 2) concretionary smithsonites in hand specimens (SK 2-St. Pierre). Mecella: (e) Hand specimen (MC) with banded smithsonite and calcite. (f) Optical microscope image (N||) showing euhedral quartz in a matrix with fluorite, associated with smithsonite from (e) (brownish parts). (g) Sample (MCN) consisting of quartz and smithsonite, which are covered by a colloform smithsonite. (h) SEM-acquired image showing fluorite and smithsonite intergrowths from (e).

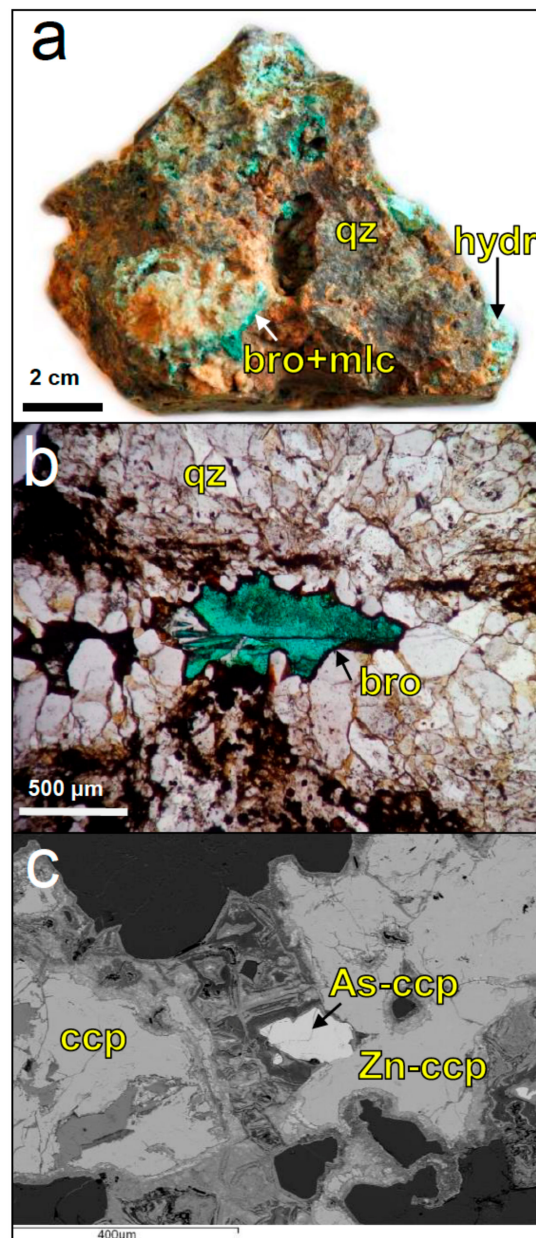


Figure 5. Jebel Azreg: (a) Hand specimen (JA). (b) Optical microscope image (N11) showing brochantite and hydrozincite intergrown with quartz. (c) Area of the sample observed by SEM (chalcopyrite with Zn and As).

The Ain Allegua analyzed sample consists of galena and sphalerite, respectively replaced by cerussite and veneers of smithsonite. Isotope analyses performed on cerussite gave a $\delta^{18}\text{O}$ value of 16.88‰ V-SMOW and a $\delta^{13}\text{C}$ value of -12.33 ‰ V-PDB (Table 2, Figure 6).

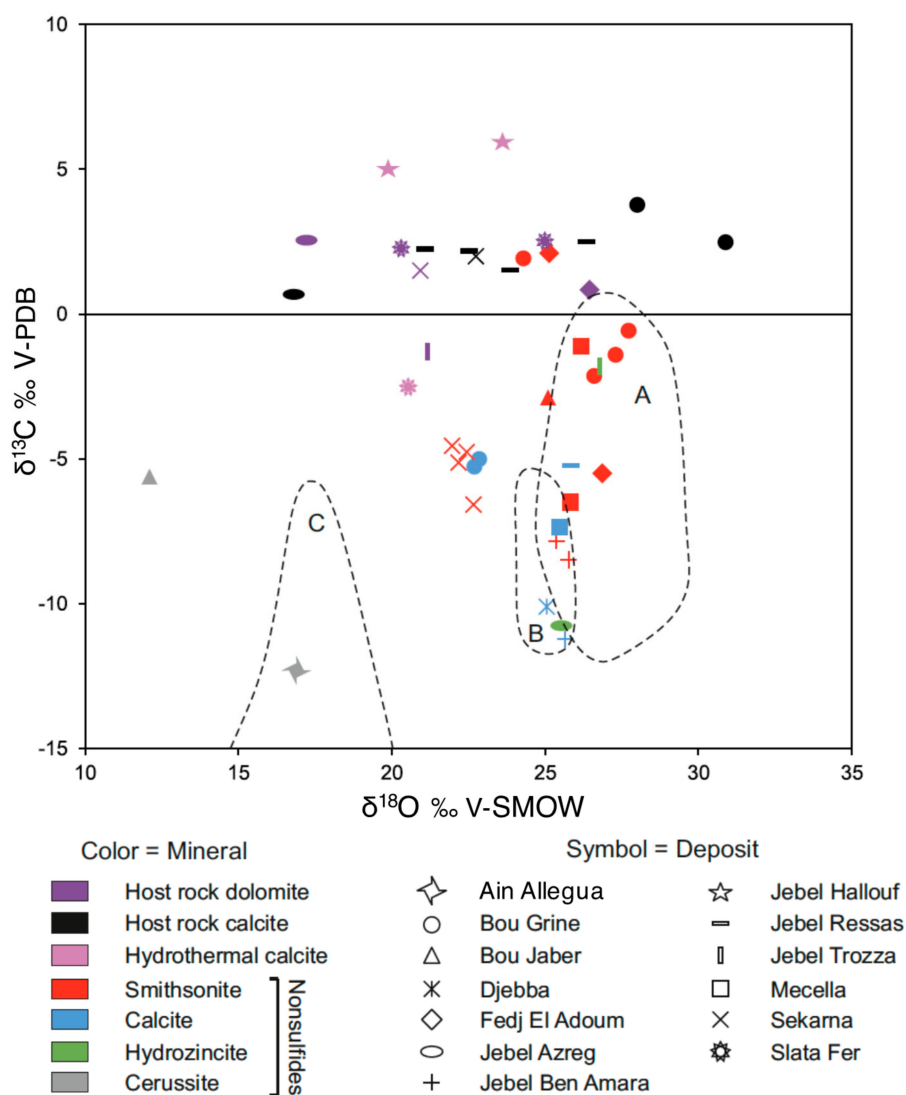


Figure 6. Carbon and oxygen isotope values of smithsonite, hydrozincite, dolomite and calcite from several occurrences in Tunisia. A, B, C indicate the supergene smithsonite, calcite and cerussite fields, respectively [67].

In the Jebel Ben Amara samples (Figure 3a), two kinds of smithsonite have been recognized: a first dark brown phase followed by a second phase of euhedral non-colored crystals (Figure 3b) and some cerussite, as well. There is a slight difference in Fe content between the two generations of smithsonite: the first smithsonite contains ~0.6 wt % FeO, whereas the second generation is pure. Calcite occurs as a late generation that follows smithsonite. Stable isotope ratios were measured on smithsonite and calcite only (Table 2; Figure 6), because cerussite was too finely intergrown to be sampled. The first type of smithsonite (dark brown) has a $\delta^{13}\text{C}$ value of -7.8‰ V-PDB, while the transparent smithsonite gives a $\delta^{13}\text{C}$ value of -8.5‰ V-PDB. The darker smithsonite has a $\delta^{18}\text{O}$ value of 25.37‰ V-SMOW, while the colorless variety has a $\delta^{18}\text{O}$ value of 25.76‰ V-SMOW. The $\delta^{13}\text{C}$ and $\delta^{18}\text{O}$ values of the late calcite are: -11.2‰ V-PDB and 25.64‰ V-SMOW, respectively.

The Jebel Hallouf analyzed sample contains galena and sphalerite, intimately associated with calcite. Thin crusts of Zn-carbonates (hydrozincite) were too small to be sampled, and the carbon and oxygen isotope ratios have been measured only on calcite. Two calcite samples show $\delta^{13}\text{C}$ values of 5.9‰ V-PDB and 5.0‰ V-PDB and $\delta^{18}\text{O}$ values of 23.60‰ V-SMOW and 19.9‰ V-SMOW (Table 2; Figure 6).

The nonsulfide samples from the Djebba deposit are earthy-looking, with their porosity filled by calcite. Goethite, hematite and the Pb-vanadate descloizite have been also identified. The $\delta^{13}\text{C}$ and $\delta^{18}\text{O}$ values of calcite are -10.1‰ V-PDB and 25.04‰ V-SMOW, respectively (Table 2; Figure 6).

From the Fedj el Adoum deposit, we analyzed two smithsonite samples (Table 2; Figure 6). The first sample (FEA ISO 1) consists of massive smithsonite replacing dolomite associated with sulfide remnants, whereas the second sample (FEA ISO 2) corresponds to a concretionary smithsonite associated with gossan-like goethite. The first smithsonite shows a $\delta^{18}\text{O}$ value of 26.86‰ V-SMOW and a $\delta^{13}\text{C}$ value of -5.50‰ V-PDB. The second smithsonite sample gave a $\delta^{18}\text{O}$ value of 25.12‰ V-SMOW and a $\delta^{13}\text{C}$ value of 2.11‰ V-PDB. The Fedj el Adoum Triassic dolomite host rock was also measured, resulting in $\delta^{13}\text{C}$ and $\delta^{18}\text{O}$ values of 0.84‰ V-PDB and 26.44‰ V-SMOW (Table 2; Figure 6).

The analyzed nonsulfide samples from the Bou Grine deposit have been collected from the upper part of the F1 orebody. The first sample is vacuolar, reddish and concretionary (Figure 3c). The other sample is brownish and concretionary too, with small calcite crystals on the surface (Figure 3e). The XRD spectra revealed in both samples the occurrence of smithsonite and calcite. Three smithsonite generations have been recognized: a first one replacing the host rock (Figure 3d) and two concretionary smithsonites, with variable Mg, Fe and Cd contents (sm2 has ~ 1.5 wt % FeO, ~ 1.7 wt % MgO and ~ 0.5 wt % Cd, whilst Sm 3 is almost stoichiometric; Figure 3d,f). The $\delta^{13}\text{C}$ composition of smithsonite (Table 2; Figure 6) ranges from -2.1 – -0.6‰ V-PDB, except that one of smithsonite Sm 3, which has a value of 1.9‰ V-PDB. The $\delta^{18}\text{O}$ values of smithsonites sm1 and sm2 range from 26.59 – 27.72‰ V-SMOW, whereas smithsonite sm3 shows a $\delta^{18}\text{O}$ value of 24.29‰ V-SMOW. Supergene calcites have $\delta^{13}\text{C}$ compositions of -5‰ and -5.27‰ V-PDB and $\delta^{18}\text{O}$ of 22.84‰ and 22.68‰ V-SMOW. The $\delta^{13}\text{C}$ and $\delta^{18}\text{O}$ values of the carbonate host rock samples (Cenomanian-Turonian Bahloul Formation) are 2.50‰ and 3.79‰ V-PDB and 30.81‰ and 27.99‰ V-SMOW, respectively.

In the Bou Jaber analyzed samples, we observed several sulfides (galena and sphalerite), associated with euhedral nonsulfide minerals (smithsonite and cerussite). In particular, cerussite occurs as mm-sized prismatic crystals in a cavity overgrowing a galena-sphalerite vein, whereas smithsonite was sampled from a crustiform sample in a cavity in the nearby host rock. Smithsonite has a $\delta^{18}\text{O}$ value of 25.09‰ V-SMOW and a $\delta^{13}\text{C}$ value of -2.87‰ V-PDB, while cerussite has $\delta^{18}\text{O}$ and $\delta^{13}\text{C}$ values of 12.09‰ V-SMOW and -5.62‰ V-PDB.

The analyzed specimen from the Sлата Fer deposit consists of fragments of botryoidal hematite, overgrown by calcite and a veneer of nonsulfide minerals (too finely intergrown to be hand-picked for isotopic analysis). A sample of the dolomite host rock has also been collected. This dolomite has $\delta^{18}\text{O}$ values of 20.3‰ and 24.98‰ V-SMOW and $\delta^{13}\text{C}$ values of 2.27‰ and 2.52‰ V-PDB. The calcite overgrowing goethite has a $\delta^{18}\text{O}$ value of 20.4‰ V-SMOW and a $\delta^{13}\text{C}$ value of -2.52‰ V-PDB.

The Jebel Trozza sample has a texture consisting of dolomite in layers, alternated with galena-quartz and hydrozincite-hematite-kaolinite veins. Traces of cerussite (not sampled) and several Pb-vanadates have also been detected. The C–O stable isotope analyses were performed on the host dolomite and on the hydrozincite veins. The $\delta^{13}\text{C}$ and $\delta^{18}\text{O}$ values of dolomite are -1.3‰ V-PDB and 21.2‰ V-SMOW. Hydrozincite shows a negative $\delta^{13}\text{C}$ (-1.8‰ V-PDB) and a strongly positive $\delta^{18}\text{O}$ (27.78‰ V-SMOW).

The nonsulfide specimens of the Sekarna ores used for this study originated from the Saint Pierre orebody. In the analyzed samples, we recognized two smithsonite types: Type 1 is a colloform yellowish aggregate (Figure 4a,b), whereas Type 2 is grey and concretionary with a white shiny crust on the surface (Figure 4c,d). Significant geochemical variations have been recognized between the two smithsonite types. Type 1 has higher Cd contents (~ 2.5 wt % CdO) than Type 2. Type 1 smithsonite has $\delta^{13}\text{C}$ ratios of -4.55‰ and -4.76‰ V-PDB and $\delta^{18}\text{O}$ ratios of 21.96‰ and 22.44‰ V-SMOW (Table 2; Figure 6). Two specimens of Type 2 smithsonite (Figure 4c,d) show $\delta^{13}\text{C}$ and $\delta^{18}\text{O}$ values of -5.13‰ and -6.57‰ V-PDB and 22.17‰ and 22.66‰ V-SMOW, respectively. Campanian-Maastrichtian limestone at Sekarna has a $\delta^{18}\text{O}$ value of 22.73‰ V-SMOW and a $\delta^{13}\text{C}$ value of 2.01‰ V-PDB. Isotope analyses of the Eocene

dolomite host rock give $\delta^{13}\text{C}$ and $\delta^{18}\text{O}$ values of 1.50‰ V-PDB and 22.73‰ V-SMOW, respectively (Table 2; Figure 6).

Two nonsulfide samples have been also collected from the Mecella deposit. The first sample is porous, banded and variable in color from light grey-white to brownish (Figure 4e). The grey bands consist of smithsonite (Figure 4f), whilst the whitish bands are composed of calcite. Reddish-brown bands consist instead of a matrix of smithsonite microcrystals mixed with Fe-oxy-hydroxides and clays, containing euhedral quartz crystals (Figure 4f) and rare fluorite (Figure 4h). The second collected sample shows a colloform smithsonite overgrowing a mixed sulfide-nonsulfide assemblage (Figure 4g). Mecella smithsonite (Table 2; Figure 6) has been sampled for isotope analyses from the grey crusts of the banded specimen and from the colloform variety. Banded smithsonite is characterized by $\delta^{13}\text{C}$ and $\delta^{18}\text{O}$ values that are -1.09‰ V-PDB and 26.17‰ V-SMOW, respectively. The associated calcite has a $\delta^{13}\text{C}$ value of -7.34‰ V-PDB and a $\delta^{18}\text{O}$ value of 25.46‰ V-SMOW. Colloform smithsonite has a $\delta^{13}\text{C}$ value of -6.49‰ V-PDB and a $\delta^{18}\text{O}$ value of 25.83‰ V-SMOW.

At Jebel Ressay, we analyzed a reddish-brown sample composed of calcite, quartz, hemimorphite and Zn-bearing clays, associated with galena remnants that are partly replaced by cerussite. Calcite appears to have replaced euhedral crystals of the original dolomite. Stable isotope analyses have been carried out on calcite veins and on the limestone host rock. Calcite veins have $\delta^{13}\text{C}$ and $\delta^{18}\text{O}$ values of -5.22‰ V-PDB and 25.83‰ V-SMOW. The host rock associated with the calcite veins is characterized by $\delta^{13}\text{C}$ and $\delta^{18}\text{O}$ values of 1.53‰ V-PDB and 23.84‰ V-SMOW, respectively. Carbon and oxygen isotope analyses, conducted on the Jurassic carbonate rock (JRH and LC samples), not directly in contact with the mineralization, allowed obtaining $\delta^{13}\text{C}$ and $\delta^{18}\text{O}$ values comprised between 2.20‰ and 2.51‰ V-PDB and 21.06‰ and 26.33‰ V-SMOW.

The Jebel Azreg sample is a massive limestone, locally dolomitized, containing sulfides altered and replaced by secondary oxidized minerals (Figure 5a). In particular, we detected chalcopyrite and mixed Pb-Zn sulfides, cut by quartz veins, altered to emerald-green brochantite and malachite, and whitish hydrozincite (Figure 5a–c). Fan-shaped aggregates of hemimorphite crystals and Ag-chlorides have also been recognized. Host rock limestone at Jebel Azreg has a $\delta^{13}\text{C}$ value of 0.69‰ V-PDB and a $\delta^{18}\text{O}$ value of 16.79‰ V-SMOW. The $\delta^{13}\text{C}$ and $\delta^{18}\text{O}$ results obtained from dolomitized host rock are 2.55‰ V-PDB and 17.21‰ V-SMOW, respectively. The $\delta^{13}\text{C}$ and $\delta^{18}\text{O}$ ratios obtained from hydrozincite are -10.76‰ V-PDB and 25.52‰ V-SMOW (Table 2; Figure 6).

6. Discussion

The Alpine orogeny during the Tertiary played a fundamental role in giving the Tunisian territory its current aspect. The collision between Africa and Europe started about 92 Ma ago [68] defining three main structural domains in northern Africa: the Atlas Chain, the Sahara Platform and the Tell-Rif foreland fold-and-thrust belt. The sulfide Zn-Pb ore deposits, which are considered Mississippi Valley-type mineralizations, are genetically related to Tunisian Alpine tectonics [1–3]. Some of the Miocene-hosted ores are also considered sediment-hosted massive sulfide (SHMS)-type Zn-Pb deposits by [69]. In the most surficial parts, several Tunisian Zn-Pb deposits present associations of sulfide and nonsulfide minerals. Considering the tectonic and metallogenic evolution of the region [1–3] and its climatic history [26], it could be considered that the Tunisian nonsulfide mineralizations have formed through sulfide weathering since the middle Miocene-late Miocene interval, when uplift-related erosion (e.g., “post-nappe” shortening phase) was able to produce sulfide uncapping and alteration (e.g., “Zeit Wet Phase”; [27]). Alteration and supergene oxidized minerals formation likely continued during the Pliocene and between the late Pleistocene and Holocene, during the onset of some relatively wet climatic periods, creating a favorable environment for weathering of sulfides (e.g., “African Humid Period”; [34,35]) and locally also under semi-arid to arid climates [70].

In the studied nonsulfide samples, the analyzed smithsonites, hydrozincites, cerussites and late calcites have variable C–O isotopes compositions. Specifically, even though the considered deposits are widespread throughout northern Tunisia and occur at different elevations and latitudes, $\delta^{13}\text{C}$ and

$\delta^{18}\text{O}$ compositions of the carbonate minerals from Ain Allegua and Jebel Ben Amara (Nappe Zone), Bou Jaber, Bou Grine and Fedj el Adoum (Diapir Zone), Mecella and Jebel Azreg (North South Zone) are comprised by a quite small field and are roughly similar to the isotopic ratios of supergene carbonates reported by [10,67]. On the contrary, the smithsonites sampled at Sekarna (Graben Zone), one smithsonite from Fedj el Adoum, one smithsonite from Bou Grine (Diapir Zone) and the cerussite sampled at Bou Jaber (Diapir Zone) have different compositions from those of typical supergene carbonates [10,67]. After [67], it is possible to use the smithsonite-water and cerussite-water oxygen isotope fractionation equations:

$$1000 \ln \alpha_{\text{smithsonite-water}} = 3.10 (10^6/T^2) - 3.50 \quad (1)$$

$$1000 \ln \alpha_{\text{cerussite-water}} = 2.29 (10^6/T^2) - 3.56 \quad (2)$$

to determine the relationships between temperature and isotopic composition of the fluids from which the carbonate minerals precipitated. The most favorable atmospheric temperatures for the formation of supergene nonsulfide deposits are commonly comprised between 15 and 25 °C (e.g., [67,69,70]), which are compatible with the climate persisting in northern Tunisia during the intervals of time (middle Miocene-late Miocene, Pliocene, late Pleistocene and Holocene (e.g., [71,72])), which can be supposed to be the most favorable periods for sulfide weathering and nonsulfide deposition. If carbonate minerals from Ain Allegua and Jebel Ben Amara (Nappe Zone), Bou Jaber, Bou Grine and Fedj el Adoum (Diapir Zone), Mecella and Jebel Azreg (North South Zone) precipitated from meteoric or groundwaters having temperatures corresponding to above the “atmospheric” range (15 and 25 °C), $\delta^{18}\text{O}$ compositions of the fluids were -7.3 – -5.5 ‰ V-SMOW at Ain Allegua, -9.1 – -6 ‰ V-SMOW at Jebel Ben Amara and Bou Jaber, -9.8 – -4.1 ‰ V-SMOW at Bou Grine and Fedj el Adoum and -8.3 – -5.6 ‰ V-SMOW at Mecella and Jebel Azreg (Figure 7). These values are similar to the compositions of modern meteoric and groundwaters in the studied localities, which range from -8 – -4 ‰ V-SMOW [73,74], thus supporting the supergene nature of the ancient fluids, which precipitated the carbonates in the various districts. This is also confirmed by the negative carbon isotope compositions of the analyzed carbonates. In fact, as pointed out by [67], negative $\delta^{13}\text{C}$ ratios can reflect: (1) values of soil carbon, when supergene alteration took place and (2) an involvement of meteoric-surficial waters with a deep and thermal circulation. A mixing between carbonate carbon from the host rock and the soil gas/atmospheric CO_2 likely occurred in all the deposits mentioned above.

Several distinct considerations must be made for the carbonates that have C–O isotope ratios outside the supergene compositional fields described by [67]. Specifically, the Bou Grine and Fedj el Adoum smithsonites, characterized by positive $\delta^{13}\text{C}$ values of 1.92‰ and 2.11‰ V-PDB and $\delta^{18}\text{O}$ compositions of 24.29‰ and 25.12‰ V-SMOW, respectively, share the common feature of being late phase in the paragenesis of the studied samples (Fedj el Adoum smithsonite is also associated with a gossan-like goethite). Considering that they have O-isotope ratios compatible with those of other supergene carbonates, their carbon-isotope ratios that exclude any contribution from soil or organic carbon could be compatible with a precipitation in drier environments, characterized by the absence of soil and vegetation. A dry (temperate to semi-arid) climate was established in the study area at the end of Pleistocene [28,31–33]. For this reason, the late position in the paragenesis of the Bou Grine and Fedj el Adoum smithsonites characterized by positive $\delta^{13}\text{C}$, suggests that the two carbonates precipitated at the end of the wet climatic stages in the two localities, after the formation of the main nonsulfide orebodies.

Looking also at the genesis of Bou Grine smithsonites in light of the geological history of the Miocene in the Diapir Zone, we might also argue that the different oxygen isotopic signatures between the early (sm1 and sm2) and late (sm3) smithsonite generations are related to different phases of structuration of the Tellian Atlas [68]. In particular, considering that the deposition of the primary Zn-Pb mineralization at Bou Grine occurred probably during the Middle Miocene and that the Pleistocene-Quaternary period was too dry for an effective deep sulfide oxidation, the first two

smithsonite generations formed in response to the early stages of the Miocene wet phases, whereas the last smithsonite generation formed during the Late Miocene to Pliocene “post-nappe” shortening phases of the Tellian chain, when a further uplift produced a change of the O-isotope composition of the meteoric waters and consequently also of the precipitating fluids.

The carbon and oxygen isotopic composition of cerussite from Bou Jaber is outside the supergene cerussite field of [67], and in particular, its $\delta^{18}\text{O}$ composition is shifted toward O-isotope ratios characteristic of a hydrothermal genesis. In addition, the wide offset of $\sim 12.7\text{‰}$ V-SMOW between the composition of this Pb-mineral and the smithsonite collected in the same deposit is incompatible with a single supergene precipitation event for both minerals (i.e., the offset values must be of $\sim 9.2\text{‰}$ V-SMOW). In the Diapir Zone, where Bou Jaber is located, there are several hot springs associated with a high geothermal gradient, with present waters with $\delta^{18}\text{O}$ values comprised between -3‰ and -4‰ V-SMOW [73]. If we assume that the Bou Jaber cerussite was precipitated from a fluid with a composition analogous to the ratios of the modern groundwaters in the region, the resulting temperature of the precipitating fluid would be ca. $55\text{--}60\text{ °C}$. This observation probably confirms that Bou Jaber cerussite has a hydrothermal origin and was likely formed from oxidizing fluids shortly after the deposition of the primary sulfides.

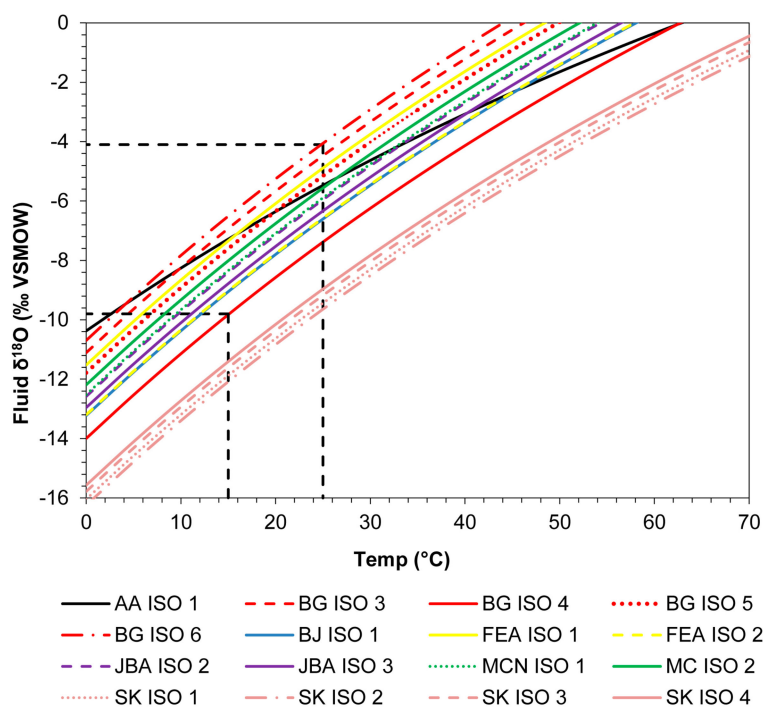


Figure 7. Fluid $\delta^{18}\text{O}$ vs. temperature ($^{\circ}\text{C}$) equilibrium curves for the analyzed smithsonite and supergene cerussite (AA ISO 1) occurring in the studied deposits. Dotted black lines evidence the $\delta^{18}\text{O}$ compositional range of the precipitating fluids, corresponding to the “typical” atmospheric temperature range (15 and 25 °C) existing during the formation of supergene deposits.

Interesting is also the case of the two distinct nonsulfide orebodies occurring in the Sekarna area, because the C–O isotope compositions of the Saint Eugène smithsonites reported by [47] ($\delta^{13}\text{C} = -5.1\text{‰}$ V-PDB and $\delta^{18}\text{O} = 28.3\text{‰}$ V-SMOW, respectively) are similar to those of other supergene carbonates mentioned in this study, whereas the smithsonite samples from the Saint Pierre orebody (analyzed in this study) are clearly different from supergene smithsonites, showing a $\delta^{13}\text{C}$ ranging from $-6.6\text{--}-4.6\text{‰}$ V-PDB and $\delta^{18}\text{O}$ from $22\text{--}22.7\text{‰}$ V-SMOW. At first instance, the diversity in the O-isotopic values of Sekarna smithsonite speaks to two separate mineralizing events concerning the Saint Eugène and Saint Pierre deposits. Secondly, the Saint Pierre smithsonite has an O-composition

incompatible with a supergene fluid. In fact, if we assume that the O-composition of the precipitating fluids was analogous to modern groundwaters in the Sekarna area ($\delta^{18}\text{O}$ composition of -6.7‰ V-SMOW; [75]) or similar to those having precipitated smithsonites in other Tunisian deposits (average $\delta^{18}\text{O}$ composition of -7‰ V-SMOW), by using the smithsonite-water fractionation equation of [67], we obtain an average precipitation temperature of ca. 40 °C , which is incompatible with a precipitation related to supergene processes. However, an explanation for high precipitation temperatures may be given if the formation of the Saint Pierre orebody was due to a mineralizing event genetically related to the geothermal activity occurring throughout central and northern Tunisia in connection with the evolution of Quaternary grabens [76], revealed in the Sekarna region through the occurrence of several thermal springs with temperatures around 40 °C and of the local anomalous geothermal gradient of 40 °C/km [77]. Considering this setting, it is likely that the Saint Pierre smithsonites formed from hot groundwaters related to the anomalous geothermal gradient existing in the area, whereas the Saint Eugène smithsonites [47] formed after supergene processes, as the smithsonites occurring in other nonsulfide deposits in Tunisia.

In addition, it must be said that all the analyzed supergene calcites (Table 2) have O-isotopic compositions incompatible with a co-precipitation of these carbonates with the smithsonites or cerussites occurring in the same deposits. Consequently, all of the analyzed supergene calcites must be considered to have formed during other episodes of weathering and/or fluids circulation occurred in the studied localities. C–O isotope compositions of the analyzed host rocks are analogues to those previously measured by other authors [4,5,41,42,47,56] and evidence a local hydrothermal modification of the original sedimentary limestones and dolostones.

7. Conclusions

In conclusion, the most common minerals in Tunisian nonsulfide deposits are smithsonite, cerussite and hydrozincite. In the studied nonsulfide samples, the analyzed smithsonites, hydrozincites, cerussites and late calcites have variable C–O isotopes compositions. Specifically, $\delta^{13}\text{C}$ and $\delta^{18}\text{O}$ compositions of the carbonate minerals from Ain Allegua and Jebel Ben Amara (Nappe Zone), Bou Jaber, Bou Grine and Fedj el Adoum (Diapir Zone), Mecella and Jebel Azreg (North South Zone) are compatible with a supergene genesis. The alteration processes that controlled the supergene oxidation of these deposits may have started in the Middle to Late Miocene and have continued through the Pliocene and between the middle Pleistocene to the Holocene.

Among the studied deposits, the smithsonites sampled at Sekarna (Graben Zone) and the cerussite sampled at Bou Jaber (Diapir Zone) have distinct C–O isotope compositions, compatible with a genesis completely different from the other deposits. In fact, the O isotopes' ratios suggest that Sekarna smithsonites precipitated from hot groundwaters related to the anomalous geothermal gradient occurring in the area, whereas the Bou Jaber cerussite probably formed from oxidizing fluids shortly after the deposition of the hypogene sulfides.

Acknowledgments: The authors are indebted to the two anonymous reviewers for discussion and help. This research was carried out with departmental funds (University of Napoli Federico II) to Maria Boni and Nicola Mondillo.

Author Contributions: Hechmi Garnit, Salah Bouhleb and Maria Boni conceived the research; Michael Joachimski, Giuliana Buongiovanni and Giuseppina Balassone carried out laboratory and analytical work; Maria Boni, Giuseppe Arfè and Nicola Mondillo analyzed the data and wrote the paper.

Conflicts of Interest: The authors declare no conflict of interest.

References

1. Rouvier, R.; Perthuisot, V.; Mansouri, A. Pb-Zn deposits and salt bearing diapirs in Southern Europe and North Africa. *Econ. Geol.* **1985**, *80*, 666–687. [[CrossRef](#)]
2. Sheppard, S.M.F.; Charef, A.; Bouhlel, S. Diapirs and Zn-Pb mineralization: A general model based on Tunisian (N. Africa) and Gulf Coast (USA) deposits. *Carbonate-Hosted Lead-Zinc Depos. Soc. Econ. Geol.* **1996**, *4*, 230–243.
3. Bouhlel, S. Carbonate hosted Mississippi Valley-type Pb-Zn deposits in Tunisia (Eastern Atlasic Belt). In *Mineral Deposit Research: Meeting the Global Challenge, Proceedings of the Eighth Biennial SGA Meeting, Beijing, China, 18–21 August 2005*; Mao, J., Bierlein, F.P., Eds.; Springer: Berlin/Heidelberg, Germany, 2005; Volume 3, pp. 19–22.
4. Bouhlel, S.; Leach, D.L.; Johnson, C.A.; Lehmann, B. Ore Textures and Isotope Signatures of the Peridiapiric Carbonate-Hosted Pb-Zn deposit of Bougrine, Tunisia. In *Proceedings of the 10th Biennial Meeting of the Society for Geology Applied to Mineral Deposits, Townsville, Australia, 17–20 August 2009*; Volume 1, pp. 409–412.
5. Bouhlel, S.; Leach, D.L.; Johnson, C.A.; Marsh, E.; Salmi-Laouar, S.; Banks, D.A. A salt diapir-related Mississippi Valley-type deposit: the Bou Jaber Pb-Zn-Ba-F deposit, Tunisia: Fluid inclusion and isotope study. *Miner. Depos.* **2016**, *51*, 749–780. [[CrossRef](#)]
6. Gottis, C.; Sainfeld, P. Les Gites Métallifères Tunisiens. In *Proceedings of the XIXème Congrès Géologique International, Alger, Algeria, September 1952*; p. 104.
7. Sainfeld, P. Les gîtes plombo-zincifères de Tunisie. *Ann. Min. Géol. Tunis* **1952**, *9*, 258.
8. Sainfeld, P. The lead-zinc-bearing deposits of Tunisia. *Econ. Geol.* **1956**, *51*, 150–177. [[CrossRef](#)]
9. Bouhlel, S.; Fortuné, J.P. Contribution à l'étude minéralogique et géochimique des minéraux de Pb-Zn-Cu de la province fluorée tunisienne. *Notes Serv. Géol. Tunis* **1985**, *51*, 155–176.
10. Boni, M.; Mondillo, N. The “Calamines” and the “Others”: The great family of supergene nonsulfide zinc ores. *Ore Geol. Rev.* **2015**, *67*, 208–233. [[CrossRef](#)]
11. Bouaziz, S.; Barrier, E.; Soussi, M.; Turki, M.M.; Zouari, H. Tectonic evolution of the northern African margin in Tunisia from paleostress data and sedimentary record. *Tectonophysics* **2002**, *3571*, 227–253. [[CrossRef](#)]
12. Burollet, P.F. Structures and tectonics of Tunisia. *Tectonophysics* **1991**, *195*, 359–369. [[CrossRef](#)]
13. Turki, M.M. Polycinématique et Contrôle Sédimentaire Associé sur la Cicatrice Zaghuan-Nebhana. Ph.D. Thesis, Faculty of Sciences of Tunis, Tunis, Tunisia, 1985.
14. Nicholson, S. The nature of rainfall variability over Africa on time scales of decades to millennia. *Glob. Planet Chang.* **2000**, *26*, 137–158. [[CrossRef](#)]
15. Janowiak, J. An investigation of interannual rainfall variability in Africa. *J. Clim.* **1988**, *1*, 240–255. [[CrossRef](#)]
16. Semazzi, F.; Mehta, V.; Sud, Y. An investigation of the relationship between sub-Saharan rainfall and global sea surface temperatures. *Atmos. Ocean* **1988**, *26*, 118–138. [[CrossRef](#)]
17. Feakins, S.J.; de Menocal, P.B. Global and African regional climate during the Cenozoic. In *Cenozoic Mammals of Africa*; Werdelin, L., Sanders, W.J., Eds.; University of California Press: Berkeley, CA, USA, 2010; pp. 45–55.
18. Hurrell, J.W. Decadal trends in the North Atlantic Oscillation: Regional temperatures and precipitation. *Science* **1995**, *269*, 676–679. [[CrossRef](#)] [[PubMed](#)]
19. Knippertz, P.; Ulbrich, U.; Marques, F.; Corte-Real, J. Decadal changes in the link between El Niño and springtime North Atlantic oscillation and European–North African rainfall. *Int. J. Climatol.* **2003**, *23*, 1293–1311. [[CrossRef](#)]
20. Dansgaard, W.S.; Johnsen, S.; Glausen, H.B.; Dahl-Jensen, D.; Gundestrup, N.S.; Hammer, C.U.; Hvidberg, C.S.; Steffesen, J.; Sveinbjörnsdóttir, A.E.; Jouzel, J.; et al. Evidence for general instability of past climate from a 250-kyr ice core record. *Nature* **1993**, *364*, 218–220. [[CrossRef](#)]
21. Stott, L.; Kennen, J.P. Antarctic Paleogene planktonic foraminifer biostratigraphy, ODP Leg 113, Sites 689 and 690. In *Proceedings of the Ocean Drilling Program, Scientific Results, Los Angeles, CA, USA, 1990*; Volume 113, pp. 549–569.
22. Le Houerou, H. Climate, flora and fauna changes in the Sahara over the past 500 million years. *J. Arid. Environ.* **1997**, *37*, 619–647. [[CrossRef](#)]
23. Bolle, M.P.; Adatte, T.; Keller, G.; Von Salis, K.; Burns, S. The Paleocene-Eocene transition in the southern Tethys (Tunisia): Climatic and environmental fluctuations. *Bull. Soc. Géol. Fr.* **1999**, *170*, 661–680.

24. Flower, B.P.; Kennett, J.P. The middle Miocene climatic transition: East Antarctica ice sheet development, deep ocean circulation and global carbon cycling. *Palaeogeogr. Palaeoclimatol. Palaeoecol.* **1994**, *108*, 537–555. [[CrossRef](#)]
25. Zachos, J.; Pagani, M.; Sloan, L.; Thomas, E.; Billups, K. Trends, rhythms, and aberrations in global climate 65 Ma to present. *Science* **2001**, *292*, 686–693. [[CrossRef](#)] [[PubMed](#)]
26. John, C.M.; Mutti, M.; Adatte, T. Mixed carbonate-siliciclastic record on the North African margin (Malta)—Coupling of weathering processes and mid Miocene climate. *Geol. Soc. Am. Bull.* **2003**, *115*, 217–229. [[CrossRef](#)]
27. Griffin, D.L. Aridity and humidity: two aspects of the late Miocene climate of North Africa and the Mediterranean. *Palaeogeogr. Palaeoclimatol. Palaeoecol.* **2002**, *182*, 65–91. [[CrossRef](#)]
28. Dupont, L.; Leroy, S. Steps towards drier climatic conditions in Northwestern Africa during the Upper Pliocene. In *Paleoclimate and Evolution with Emphasis on Human Origins*; Vrba, E., Denton, G., Partridge, T., Burckle, L., Eds.; Yale University Press: New Haven, CT, USA, 1995; pp. 289–297.
29. Haywood, A.; Sellwood, B.; Valdes, P. Regional warming: Pliocene (3 Ma) paleoclimate of Europe and Mediterranean. *Geology* **2000**, *38*, 1063–1066. [[CrossRef](#)]
30. De Menocal, P.B. African climate change and faunal evolution during the Pliocene–Pleistocene. *Earth Planet Sci. Lett.* **2004**, *220*, 3–24. [[CrossRef](#)]
31. Tiedemann, R.; Sarnthein, M.; Shackleton, N.J. Astronomical timescale for the Pliocene Atlantic $\delta^{18}\text{O}$ and dust flux records of ODP Site 659. *Paleoceanography* **1994**, *9*, 619–638. [[CrossRef](#)]
32. De Menocal, P.B. Plio-Pleistocene African climate. *Science* **1995**, *270*, 53–59. [[CrossRef](#)]
33. De Menocal, P.; Bloemendal, J. Plio-Pleistocene climatic variability in subtropical Africa and the paleoenvironment of hominid evolution: A combined data-model approach. In *Paleoclimate and Evolution with Emphasis on Human Origins*; Vrba, E., Denton, G., Partridge, T., Burckle, L., Eds.; Yale University Press: New Haven, CT, USA, 1995; pp. 262–288.
34. Pokras, E.; Mix, A.C. Earth's precession cycle and Quaternary climatic change in tropical Africa. *Nature* **1987**, *326*, 486–487. [[CrossRef](#)]
35. De Menocal, P.B.; Ortiz, J.; Guilderson, T.; Adkins, J.; Sarnthein, M.; Baker, L.; Yarusinsky, M. Abrupt onset and termination of the African Humid Period: Rapid climate responses to gradual insolation forcing. *Quatern. Sci. Rev.* **2000**, *19*, 347–361. [[CrossRef](#)]
36. Haynes, C.V.; Mead, A.R. Radiocarbon dating and paleoclimatic significance of sub-fossil *Limicolaria* in NW Sudan. *Quatern. Res.* **1987**, *28*, 86–89. [[CrossRef](#)]
37. Rognon, P. Late Quaternary climatic reconstruction for the Maghreb (North Africa). *Palaeogeogr. Palaeoclimatol. Palaeoecol.* **1987**, *58*, 11–34. [[CrossRef](#)]
38. Kropelin, S.; Soulie-Marsche, I. Charophyte remains from Wadi Howar as evidence for deep mid-Holocene freshwater lakes in the eastern Sahara of northwest Sudan. *Quatern. Res.* **1991**, *36*, 210–223. [[CrossRef](#)]
39. Bouhleb, S. *Gitologie, Minéralogie et Essai de Modélisation des Minéralisations à F-Ba-Sr-Pb-Zn-(S) Associées aux Carbonates (Jurassiques et Cretacés) et aux Diapirs Triasiques: Gisements de Stah-Kohol, Zriba-Guebli, Bou Jaber et Fej Lahdoum (Tunisie Septentrionale)*. Ph.D. Thesis, Sciences Géologiques, Université de Tunis, Tunis, Tunisian Republic, 1993; p. 293.
40. Decrée, S.; Marignac, C.; De Putter, T.; Deloule, E.; Liégeois, J.P.; Demaiffe, D. Pb-Zn mineralization in a Miocene regional extensional context: The case of the Sidi Driss and the Douahria ore deposits (Nefza mining district, Northern Tunisia). *Ore Geol. Rev.* **2008**, *34*, 285–303. [[CrossRef](#)]
41. Bouhleb, S.; Johnson, C.A.; Leach, D.L. The peridiapiric-type Pb–Zn deposit at Fedj El Adoum, Tunisia: geology, petrography, and stable isotopes. In *Proceedings of the Ninth Biennial SGA Meeting, Dublin, Ireland, 20–23 August 2007*; pp. 323–325.
42. Orgeval, J.J. Peridiapiric metal concentration: Example of the Bou Grine deposit (Tunisian Atlas). In *Sediment-Hosted Zn-Pb Ores*; Springer: Berlin/Heidelberg, Germany, 1994; pp. 354–389.
43. Schmidt, S.C. Re-activation of the Bougrine Mine, Tunisia. In *Proceedings of the 101st Annual General Meeting of the Canadian Institute Mining, Metallurgy and Petroleum-Mining, Calgary, AB, Canada, May 1999*.
44. Bejaoui, J.; Bouhleb, S.; Sellami, A.; Braham, A. Geology, mineralogy and fluid inclusion study of Oued Jebb Pb–Zn–Sr deposit; comparison with the Bou Grine deposit (diapirs zone, Tunisian atlas). *Arab. J. Geosci.* **2014**, *7*, 2483–2497. [[CrossRef](#)]

45. Jrad, L.; Perthuisot, V. Diapirisme, orogénèse et minéralisation Pb-Zn en Afrique du Nord: Exemple des gisements du J. Ajred et du J. Hamra en Tunisie centrale. *C. R. Acad. Sci. Paris* **1995**, *321*, 721–728.
46. Bejaoui, J.; Bouhlef, S.; Cardellach, E.; Canals, À.; Perona, J.; Piqué, À. Mineralization and fluid inclusion studies of the Aptian carbonate-hosted Pb-Zn-Ba ore deposits at Jebel Hamra. Central Tunisia. *J. Geochem. Explor.* **2013**, *128*, 136–146. [[CrossRef](#)]
47. Garnit, H.; Bouhlef, S.; Barca, D.; Johnson, C.A.; Chtara, C. Phosphorite-hosted zinc and lead mineralization in the Sekarna deposit (Central Tunisia). *Miner. Deposita* **2012**, *47*, 545–562. [[CrossRef](#)]
48. Rouvier, R. Géologie de L'extrême-Nord Tunisien: Tectoniques et Paléogéographies Superposées à L'extrémité Orientale de la Chaîne Nord-Maghrebine. Ph.D. Thesis, Université Pierre et Marie Curie, Paris, France, 1977.
49. Martinez, C.; Truillet, R. Evolution paléogéographique et structurale de la Tunisie. *Mem. Soc. Geol. It.* **1987**, *38*, 35–45.
50. Ben Ayed, N. Évolution tectonique de L'avant-Pays de la Chaîne Alpine de Tunisie du Début du Mésozoïque à l'Actuel. Ph.D. Thesis, Université Paris Sud-Paris XI, Paris, France, 1986.
51. Chihî, L. Les Fossés Néogènes à Quaternaires de la Tunisie et de la mer Pélagienne: Leur Étude Structurale et Leur Signification Dans le Cadre Géodynamique De La Méditerranée Centrale. Ph.D. Thesis, Université Tunis II, Tunis El Manar, Tunisia, 1995; p. 566.
52. Rouvier, R. Minéralisations plombo-zincifères et phénomène karstique. Exemple tunisien: Le gisement du Djebel Hallouf. *Miner. Deposita* **1971**, *6*, 196–206. [[CrossRef](#)]
53. Mansouri, A. Gisements de Pb-Zn et Karstification en Milieu Continental: Le District Minier du Djebel Hallouf-Sidi Bou Aouane (Tunisie septentrionale). Ph.D. Thesis, Université Pierre et Marie Curie, Paris, France, 1980.
54. Charef, A. La nature et le rôle des phases fluides associées à la minéralisation Pb-Zn dans les formations carbonatées et leurs conséquences métallogéniques: études des inclusions fluides et des isotopes (H, C, O, S, Pb) des gisements des Malines (France), Jebel Hallouf-Sidi Bou Aouane et Fedj-el-Adoum (Tunisie). Ph.D. Thesis, Université Nancy, Nancy, France, 1986.
55. Mohamed-Naceur, M. Étude de Minéralisations Vanadifères dans les Poches Karstiques du Jebel Goraa (Djebba-Tunisie). Ph.D. Thesis, Université de Paris-Sud, Orsay, France, 1973.
56. Charef, A.; Sheppard, S.M. Pb-Zn mineralization associated with diapirism: Fluid inclusion and stable isotope (H, C, O) evidence for the origin and evolution of the fluids at Fedj-el-Adoum, Tunisia. *Chem. Geol.* **1987**, *61*, 113–134. [[CrossRef](#)]
57. Perthuisot, V. Diapirism in northern Tunisia. *J. Struct. Geol.* **1981**, *33*, 231–235. [[CrossRef](#)]
58. Floridia, S. La province fluorée tunisienne. Aperçu géologique et métallogénique. Livre jubilaire M. Solignac. *Ann. Min. Géol. Tunis.* **1973**, *2*, 477–479.
59. Thibieroz, J. Hammam Jedidi et Hammam Zriba: Etude Géologique et Minière de Deux Gisements Stratiformes Dans le Cadre de la Province Fluorée Tunisienne; L'association des Concentrations Fluorées Aux Surfaces D'émergence. Master's Thesis, Université Paris VI, Paris, France, 1974.
60. Jemmali, N.; Souissi, F.; Vennemann, T.W.; Carranza, E.J.M. Genesis of the Jurassic Carbonate-Hosted Pb-Zn deposits of Jebel Ressas (North-Eastern Tunisia): Evidence from Mineralogy, Petrography and Trace Metal Contents and Isotope (O, C, S, Pb) Geochemistry. *Res. Geol.* **2011**, *61*, 367–383. [[CrossRef](#)]
61. Souissi, F.; Dandurand, J.L.; Fortune, J.P. Thermal and chemical evolution of fluids during fluorite deposition in the Zaghuan province, north-eastern Tunisia. *Miner. Deposita* **1997**, *32*, 257–270. [[CrossRef](#)]
62. Morgan, M.A.; Grocott, J.; Moody, R.T. The structural evolution of the Zaghuan-Ressas structural belt, northern Tunisia. *Geol. Soc. Lond. Spec. Publ.* **1998**, *132*, 405–422. [[CrossRef](#)]
63. Souissi, F.; Jemmali, N.; Souissi, R.; Dandurand, J.L. REE and isotope (Sr, S, and Pb) geochemistry to constrain the genesis and timing of the F-(Ba-Pb-Zn) ores of the Zaghuan district (NE Tunisia). *Ore Geol. Rev.* **2013**, *55*, 1–12. [[CrossRef](#)]
64. Kim, S.T.; Mucci, A.; Taylor, B.E. Phosphoric acid fractionation factors for calcite and aragonite between 25 and 75 °C: Revisited. *Chem. Geol.* **2007**, *246*, 135–146. [[CrossRef](#)]
65. Rosenbaum, J.; Sheppard, S.M. An isotopic study of siderites, dolomites and ankerites at high temperatures. *Geochim. Cosmochim. Acta* **1986**, *50*, 1147–1150. [[CrossRef](#)]
66. Gilg, H.A.; Struck, U.; Vennemann, T.; Boni, M. Phosphoric acid fractionation for smithsonite and cerussite between 25 and 72 °C. *Geoch. Cosmochim. Acta* **2003**, *67*, 4049–4055. [[CrossRef](#)]

67. Gilg, H.A.; Boni, M.; Hochleitner, R.; Struck, U. Stable isotope geochemistry of carbonate minerals in supergene oxidation zones of Zn–Pb deposits. *Ore Geol. Rev.* **2008**, *33*, 117–133. [[CrossRef](#)]
68. De Lamotte, D.F.; Saint Bezar, B.; Bracène, R.; Mercier, E. The two main steps of the Atlas building and geodynamics of the western Mediterranean. *Tectonics* **2000**, *19*, 740–761. [[CrossRef](#)]
69. Decrée, S.; Marignac, C.; Abidi, R.; Jemmali, N.; Deloule, E.; Souissi, F. Tectonomagmatic Context of Sedex Pb–Zn and Polymetallic Ore Deposits of the Nappe Zone Northern Tunisia, and Comparisons with MVT Deposits in the Region. In *The Mineral Deposits of North Africa*; Springer: Berlin/Heidelberg, Germany, 2016; pp. 497–525.
70. Reichert, J.; Borg, G. Numerical simulation and a geochemical model of supergene carbonate-hosted nonsulphide zinc deposits. *Ore Geol. Rev.* **2008**, *33*, 134–151. [[CrossRef](#)]
71. Bruch, A.; Uhl, D.; Mosbrugger, V. Miocene climate in Europe—Patterns and evolution: A first synthesis of NECLIME. *Palaeogeogr. Palaeoclimatol. Palaeoecol.* **2007**, *253*, 1–7. [[CrossRef](#)]
72. Desprat, S.; Combourieu-Nebout, N.; Essallami, L.; Sicre, M.A.; Dormoy, I.; Peyron, O.; Siani, G.; Bout Roumazielles, V.; Turon, J.L. Deglacial and Holocene vegetation and climatic changes in the southern Central Mediterranean from a direct land–sea correlation. *Clim. Past* **2013**, *9*, 767–787. [[CrossRef](#)]
73. Hamed, Y. Stable isotope ratios in meteoric waters in El Kef Region, Northwestern Tunisia: Implications for changes of moisture sources. *J. Earth Sci. Clim. Chang.* **2014**, *5*, 203.
74. Mejri, S.; Chekirbane, A.; Maki Tsujimura, M.; Mlayah, A.; Boughdiri, M. Tracing groundwater salinization processes in an inland aquifer: A hydrogeochemical and isotopic approach in Sminja aquifer, Northeast of Tunisia. In Proceedings of the International Conference on African Large River Basins Hydrology, Hammamet, Tunisia, 26–30 October 2015.
75. Tricart, P.; Torelli, L.; Argnani, A.; Rekhiss, F.; Zitellini, N. Extensional collapse related to compressional uplift in the Alpine Chain off northern Tunisia (Central Mediterranean). *Tectonophysics* **1994**, *238*, 317–329. [[CrossRef](#)]
76. Fourré, E.; Di Napoli, R.; Aiuppa, A.; Parello, F.; Gaubi, E.; Jean-Baptiste, P.; Allard, P.; Calabrese, S.; Mamou, A.B. Regional variations in the chemical and helium-carbon isotope composition of geothermal fluids across Tunisia. *Chem. Geol.* **2011**, *288*, 67–85. [[CrossRef](#)]
77. Dhia, H.B. The geothermal gradient map of central Tunisia: comparison with structural, gravimetric and petroleum data. *Tectonophysics* **1987**, *142*, 99–109. [[CrossRef](#)]



© 2018 by the authors. Licensee MDPI, Basel, Switzerland. This article is an open access article distributed under the terms and conditions of the Creative Commons Attribution (CC BY) license (<http://creativecommons.org/licenses/by/4.0/>).